Effects of antidot shape on the spin wave spectra of two-dimensional $Ni_{80}Fe_{20}$ antidot lattices

Ruma Mandal, Pinaki Laha, Kaustuv Das, Susmita Saha, Saswati Barman, A. K. Raychaudhuri, and Anjan Barman

Citation: Appl. Phys. Lett. **103**, 262410 (2013);
View online: https://doi.org/10.1063/1.4860959
View Table of Contents: http://aip.scitation.org/toc/apl/103/26
Published by the American Institute of Physics

Effects of antidot shape on the spin wave spectra of two-dimensional $Ni_{80}Fe_{20}$ antidot lattices

Ruma Mandal, Pinaki Laha, Kaustuv Das, Susmita Saha, Saswati Barman, A. K. Raychaudhuri, and Anjan Barman[a)]

Thematic Unit of Excellence on Nanodevice Technology, Department of Condensed Matter Physics and Material Sciences, S. N. Bose National Centre for Basic Sciences, Block JD, Sector III, Salt Lake, Kolkata 700 098, India

(Received 5 November 2013; accepted 15 December 2013; published online 31 December 2013)

We show that the optically induced spin wave spectra of nanoscale $Ni_{80}Fe_{20}$ (permalloy) antidot lattices can be tuned by changing the antidot shape. The spin wave spectra also show an anisotropy with the variation of the in-plane bias field orientation. Analyses show this is due to various quantized and extended modes, whose nature changes with the antidot shape and bias field orientation as a result of the variation of the internal magnetic field profile. The observed variation and anisotropy in the spin waves with the internal and external parameters are important for their applications in magnonic devices. © *2013 AIP Publishing LLC*. [http://dx.doi.org/10.1063/1.4860959]

Ferromagnetic antidot lattices have emerged as a strong candidate for magneto-photonic crystals[1,2] and ultra-high density magnetic data storage media.[3] More recently, they have been studied intensively as a promising candidate for magnonic devices. Waveguides,[4] filters,[5] interferometers,[6] phase shifters,[7] spin wave logic,[8] and magnonic crystals[9,10] are some important components of magnonic devices and investigation of spin wave dispersion in such devices with their structural and material parameters is at the forefront of research in magnonics. For antidot lattices with large periods in μm and sub-μm range, inhomogeneous internal magnetic fields play important role in determining the frequencies and spatial characters of the spin waves, while for reduced period down to few tens of nm, the exchange field starts to play important role. Consequently, a large number of parameters of antidot lattices can be varied to tune the spin waves in them. These include the size and shape of the antidots, the spacing between the antidots (lattice constant), base material, and the strength and orientations of the bias magnetic field.

In this paper, we investigate the spin wave spectra in a two-dimensional antidot lattice with varying antidot shapes, namely, square, circular, triangular, and diamond shapes. When the bias field is applied parallel to one of the edges of the lattices, a remarkable difference in the spin wave spectra is observed in the lattices with triangular and diamond shaped antidots as opposed to the circular and square shaped antidots. In addition, a strong anisotropy in spin wave spectra is observed as the bias field is rotated by 45° w.r.t. the edges of the lattice. We understood this significant variation as a result of the variation in the internal field profiles surrounding the antidots and the resulting spin wave mode profiles with the aid of the micromagnetic simulations.

Initial studies on the dynamics of ferromagnetic antidot lattices showed pattern induced splitting of surface and volume modes,[11] localization, confinement, and field-controlled propagation of spin waves,[12,13] and observation of dispersive and entangled spin waves between the antidots.[14] Later, anisotropic propagation and damping of spin waves were observed due to magnetic field-controlled spin wave guiding in a network of interconnected nanowires.[15] Ulrichs *et al.* observed a field independent localized mode in CoFeB antidot lattice.[16] Effects of lattice symmetry[17] and diameters of the antidots on spin waves,[18] formation of magnonic minibands,[19] and tunable metamaterial response in permalloy antidot lattices[20] attracted great interests. Recently, a number of works reported complete magnonic bandgaps,[21] linear bias field dependence of high-symmetric magnonic modes for perpendicularly magnetized antidot lattices,[22] transformation of quantized spin waves to propagating ones by changing the in-plane orientation of magnetic field,[23] and tunable frequency gap in spin wave spectra with varying lattice constants.[24] Micromagnetic simulations showed the effects of antidot shape on magnonic bandgap in one-dimensional magnonic antidot waveguide in an exchange dominated regime.[25] However, the effects of the shapes of the antidot on the demagnetizing field profiles inside an antidot lattice and the corresponding spin wave spectra have not been extensively studied. The spin wave dispersion for a square lattice with varying shape of the basis (antidot) structure, particularly when calculated along Γ-M and X-M symmetry axes, may show anisotropy arising from symmetry considerations. However, here we measure the zero wavevector modes (i.e., at the centre of the Brillouin zone) and some dispersionless localized and standing wave modes. Hence, the demagnetizing field profiles surrounding the antidots play the major role. The dispersionless modes are the forbidden modes, forming bandgaps in the antidot lattices.

Square, circular, triangular, and diamond shaped antidots with about 200 nm width and height and having separation between the nearest edges of about 230 nm were fabricated on square lattices, each covering $10 \times 10\ \mu m^2$ area on a 20 nm thick permalloy film coated with a 5 nm SiO_2 protective layer. The circular antidots were fabricated by focused ion beam milling using liquid Ga^+ ion beam at 30 kV voltage and 28 pA beam current, which produced a spot size of about 8 nm. Since square, triangular, and diamond shapes have sharp corners, we used lower spot size (~4 nm) by reducing the beam current to 10 pA. The presence of 5 nm thick SiO_2 capping

a)Email: abarman@bose.res.in

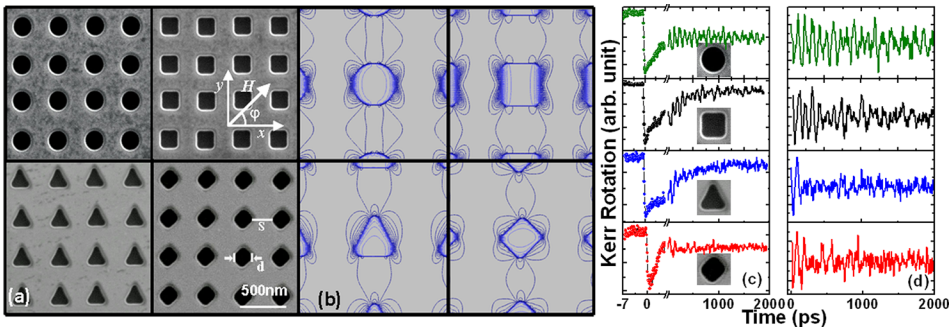

FIG. 1. (a) Scanning electron micrographs of four different antidot lattices with varying antidot shapes and (b) simulated magnetostatic fields within those lattices. (c) Time-resolved Kerr rotation from different antidot lattices showing three different temporal regimes, namely, ultrafast demagnetization, fast relaxation, and spin precession superposed on a slow relaxation and (d) the precessional part of the time-resolved Kerr rotation after a bi-exponential background subtraction.

layer protects the un-milled permalloy film to a large extent from direct irradiation, while damages at the edges of the antidots due to Ga^+ ion implantation occurring laterally are limited to only about 5 nm from the edges. Further details of the focused ion beam milling can be found elsewhere.[24] The scanning electron micrographs (Fig. 1(a)) show that the square, triangular, and diamond shaped antidots have rounded corners due to the finite size of the ion beam. The triangular and diamond shaped antidots also suffer from small asymmetry in their shapes. The antidot size and edge-to-edge separation show upto $\pm 5\%$ deviation. All the above deviations will be introduced in the numerical simulations except for the edge roughness, possible edge pinning and variation of material quality at the antidot edges because of Ga^+ ion implantation due to the difficulty in their characterization. The time-resolved magnetization dynamics was measured by an all-optical time--resolved magneto-optical Kerr effect microscope.[24] The dynamics was excited by the second-harmonic ($\lambda = 400$ nm, pulse width = 100 fs, fluence = 16 mJ/cm^2) of a Ti-sapphire oscillator (Tsunami, Spectra-Physics) with a spot size of about 1 μm. The time-delayed fundamental beam (800 nm, 70 fs, 3 mJ/cm^2) with a spot size of about 800 nm and placed at the centre of the pump beam is used to probe the dynamics by measuring the Kerr rotation as a function of the time-delay between the pump and the probe beams. Consequently, about 3×3 antidots were measured from each array. The external bias magnetic field is tilted at a small angle ($\sim 10°$) from the plane of the sample, the in-plane component of which is denoted by H in Fig. 1(a). The experimental results are reproduced by using micromagnetic simulations using OOMMF software.[26] We have studied arrays of 7×7 antidots with varying shapes and discretized the arrays into rectangular prisms with dimensions $3 \times 3 \times 20$ nm^3. Further, test simulations with larger arrays (11×11 antidots) do not show any significant difference. The shapes of the antidots are derived from the SEM images, and material parameters used in the simulations are gyromagnetic ratio, $\gamma = 17.5$ MHz/Oe, magnetocrystalline anisotropy, $H_k = 0$, saturation magnetization, $M_s = 800$ emu/cc and exchange stiffness constant, $A = 1.3 \times 10^{-6}$ erg/cm. The simulation methods are described in detail elsewhere.[24] The bias field is applied according to the experimental configurations and a pulsed field of peak value of 20 Oe, 10 ps rise/fall time and 20 ps pulse duration is used perpendicular to the sample plane, while a damping coefficient $\alpha = 0.015$ is used during dynamic simulations.

In Fig. 1(b), we show the contour plot of simulated magnetostatic field distributions for four lattices, which show the nonuniform magnetic field distributions (demagnetized regions) around the edges of the antidots. While the symmetry of the demagnetized regions is similar for the circular and square antidots, it changes significantly for the triangular and diamond shaped antidots. In addition to the nominal variation in the shape, introduction of asymmetry of shape due to fabrication defect poses further differences in the internal field profile. Figure 1(c) shows the time-resolved Kerr rotations for four samples at $H = 900$ Oe revealing three important temporal regimes, namely, the ultrafast demagnetization (500 fs), fast relaxation (5.4 ps), and precessional motion superposed on a slow relaxation (334 ps). In Fig. 1(d), we show the precessional dynamics after subtracting a bi-exponential background. The spin wave spectra are obtained by taking fast Fourier transform (FFT) of the background subtracted time-resolved Kerr rotation as shown in Fig. 2 for all four samples at three bias field orientations $\varphi = 0°$, 45°, and 90°. The spectra for $\varphi = 0°$ and 90° are qualitatively similar but there are some quantitative differences due to the fabrication induced structural asymmetry in the antidots of each shape to varying extent.

Figure 2(a) reveals that the circular and square shaped antidot lattices show two dominant bands of frequencies with a gap of about 3.17 and 3.34 GHz, respectively. For the square antidot lattice, another low amplitude shoulder is observed at about 5.9 GHz. In the triangular antidot lattice, another mode appears in the gap between the two bands,

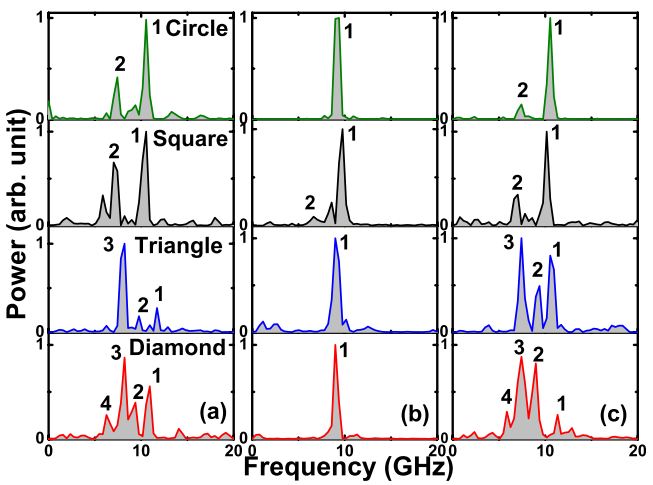

FIG. 2. Spin wave spectra obtained from experimental time-resolved Kerr rotation data from four different antidot lattices for three different bias field orientations (a) $\varphi = 0°$, (b) $\varphi = 45°$, and (c) $\varphi = 90°$.

reducing the gap to about 1.7 GHz each between the three bands. For the diamond antidot lattice, four closely spaced modes occur with narrow gaps of about 1.35, 1.25, and 1.85 GHz. We have qualitatively reproduced the observed spin wave spectra by micromagnetic simulations as shown in Fig. 3. It shows two bands of modes for the circular and square shaped antidot lattices with frequency gaps of 3.9 and 4.5 GHz, respectively. The triangular antidots lattice shows three modes with two frequency gaps of about 2.1 GHz each, between the three modes. On the other hand, the diamond shaped lattice shows four closely spaced modes with frequency gaps of 1.8, 1.8, and 1.2 GHz. The remarkable difference in the spin wave spectra between different antidot shapes stems from their internal field profiles, which lead to various extended and localized modes as shown later in this article. At $\varphi = 45°$, a strong anisotropy in the spin wave spectra with a dominant mode just below 10 GHz is observed for all lattices. For circular antidots, the mode frequency is about 9.3 GHz, which is intermediate between the two bands of modes observed for $\varphi = 0°$ and 90°. However, for the square antidots, in addition to a dominant mode at around 9.8 GHz, a small amplitude mode at 6.6 GHz is also observed. In triangular and diamond shaped antidots again a single mode at 9.1 and 9.0 GHz is observed. Dominant single mode for circular, triangular, and diamond shaped antidot lattices and an additional small amplitude mode at lower frequency for the square shaped antidot are reproduced in the simulated spectra. The simulated peak frequencies are slightly (5%–10%) higher than the experimental frequencies.

We have further simulated the profiles of the resonant modes[27] and the simulated power maps are shown in Fig. 4. At $\varphi = 0°$, mode 1 in the circular antidot lattice is a quantized mode (mode number $q = 5$) due to the formation of standing wave in the backward volume magnetostatic (BWVMS) wave geometry between two neighboring antidots. Mode 2 is an extended mode flowing through the channel between the neighboring antidots in the Damon-Eshbach (DE) geometry. In the square lattice, mode 1 is again a quantized mode, while mode 2 is identical to mode 2 of circular antidot lattice. In the triangular antidot lattice, mode 1 is also

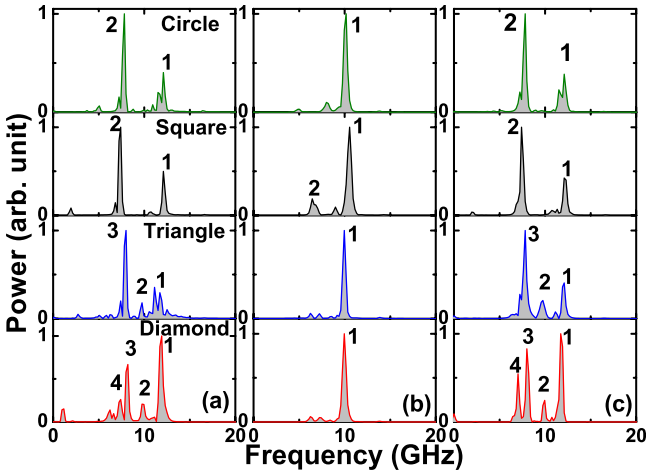

FIG. 3. Simulated spin wave spectra from four different antidot lattices for three different bias field orientations (a) $\varphi = 0°$, (b) $\varphi = 45°$, and (c) $\varphi = 90°$.

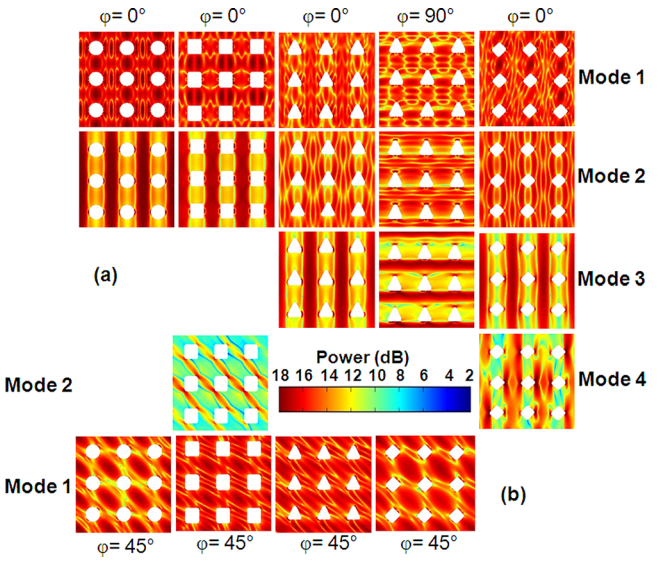

FIG. 4. Spin wave mode profile (power) for antidot lattices with varying shapes with the bias field orientation of (a) $\varphi = 0°$ or 90° and (b) $\varphi = 45°$. The colormap used for the mode profiles is shown inside the figure.

a quantized mode with $q = 5$ but in this case the standing wave does not form exactly between the two antidots but shifts down vertically and becomes asymmetric due to the asymmetry in the internal field profile. Mode 2 is a quantized mode with $q = 3$ along the bias field direction but it extends in the direction perpendicular to the bias field forming a serpentile shape through the channel between the neighboring antidots. This shape of mode also stems from the internal field profile. Mode 3 is the extended mode in the space between the antidots in the DE geometry. Unlike the other shapes of antidots, in this case, when the field is rotated by 90° mode profiles for all three modes change significantly giving rise to further differences in the frequency spectra. In the diamond shaped antidot lattice, the first three modes are identical to those of the triangular antidots with small changes in shape due to the different internal field profile. However, in this case a fourth mode appears, which is a DE-like mode that got modified by the corners of the diamond shape. The absence of the $q = 3$ mode in the circular and square antidot lattices causes larger gap in their frequency spectra, while appearance of the same reduces that gap in the triangular and diamond antidot lattices. At $\varphi = 45°$, mode 1 is identical for all antidot shapes, which is the localized (trapped) mode between the next nearest antidots perpendicular to the field direction. However, there is a small difference between different antidot shapes of the localized mode profile, which changes due to the variation in the internal field profile. For the square antidot a weak extended second mode (mode 2) in the DE geometry is accommodated in the narrow channel between the antidots, while this mode does not appear with significant amplitude in other antidot lattices, where the demagnetizing fields surrounding the neighboring antidots start to overlap at this value of φ, blocking the path of the extended spin wave mode.

In summary, we have investigated the effects of the shape of the antidots on the spin waves in permalloy antidot lattices. Significant differences in the spin wave spectra are observed with the variation in the antidot shape. Two

prominent modes with significant gaps in the spin wave spectra for the circular and square shaped antidots change into three and four closely spaced modes with narrow gaps for the triangular and diamond shaped antidot lattices, respectively. In addition, when the bias field is rotated within the sample plane by $\varphi = 45^\circ$ from the horizontal or vertical edges of the lattices, a single dominant mode is observed for three lattices except for the square shaped antidot lattice, where an additional low amplitude mode occurs at lower frequency. Micromagnetic simulations helped to identify the spin wave modes. While for the circular and square antidot lattices the higher frequency mode is a quantized mode in the BWVMS geometry with mode number $q = 5$, the lower frequency mode is an extended DE mode. In the triangular and diamond shaped antidot lattices, an additional quantized mode with $q = 3$ appeared in the frequency gap observed for the other two lattices probably due to the sharp corners concentrating the demagnetizing field and thereby providing additional pinning regions. Due to the same fields, in the diamond shaped antidot lattice another modified DE-like mode appears at frequency below the DE mode. At $\varphi = 45^\circ$, the extended DE mode disappears for the circular, triangular, and diamond shaped antidot lattices and its power is reduced significantly in the square antidot lattice, while a mode localized in the region between the next nearest antidots in a direction perpendicular to the bias field becomes dominant. The observed tunability of the spin wave spectrum with the antidot shape and the bias field orientation may give rise to an enabling tool for tuning the frequency of such devices when they are used as magnonic filters, splitters, and other magnonic devices.

We gratefully acknowledge the financial supports from Department of Science and Technology, Government of India under the Grant Nos. INT/JP/JST/P-23/09, SR/NM/NS-09/2011(G), and Department of Information Technology, Government of India under Grant No. 1(7)/2010/M&C. We also acknowledge technical helps from Dheeraj Kumar and Bivas Rana during this work. S.B. wants to acknowledge DST (Grant Nos. SR/NM/NS-53/2010 and SR/WOS-A/PS-27/2010) for financial support.

[1]K. Kern, D. Heitmann, P. Grambow, Y. H. Zhang, and K. Ploog, Phys. Rev. Lett. **66**, 1618 (1991).
[2]G. Ctistis, E. Papaioannou, P. Patoka, J. Gutek, P. Fumagalli, and M. Giersig, Nano Lett. **9**, 1 (2009).
[3]L. Torres, L. Lopez-Diaz, and O. Alejos, J. Appl. Phys. **87**, 5645 (2000).
[4]J. W. Kłos, D. Kumar, M. Krawczyk, and A. Barman, Sci. Rep. **3**, 2444 (2013).
[5]S.-K. Kim, K.-S. Lee, and D.-S. Han, Appl. Phys. Lett. **95**, 082507 (2009).
[6]J. Podbielski, F. Giesen, and D. Grundler, Phys. Rev. Lett. **96**, 167207 (2006).
[7]Y. Au, M. Dvornik, O. Dmytriiev, and V. V. Kruglyak, Appl. Phys. Lett. **100**, 172408 (2012).
[8]T. Schneider, A. A. Serga, B. Leven, B. Hillebrands, R. L. Stamps, and M. P. Kostylev, Appl. Phys. Lett. **92**, 022505 (2008).
[9]V. V. Kruglyak, S. O. Demokritov, and D. Grundler, J. Phys. D: Appl. Phys. **43**, 264001 (2010).
[10]B. Lenk, H. Ulrichs, F. Garbs, and M. Münzenberg, Phys. Rep. **507**, 107 (2011).
[11]S. McPhail, C. M. Gürtler, J. M. Shilton, N. J. Curson, and J. A. C. Bland, Phys. Rev. B **72**, 094414 (2005).
[12]S. Neusser, B. Botters, and D. Grundler, Phys. Rev. B **78**, 054406 (2008).
[13]S. Neusser, B. Botters, M. Becherer, D. Schmitt-Landsiedel, and D. Grundler, Appl. Phys. Lett. **93**, 122501 (2008).
[14]M. Kostylev, G. Gubbiotti, G. Carlotti, G. Socino, S. Tacchi, C. Wang, N. Singh, A. O. Adeyeye, and R. L. Stamps, J. Appl. Phys. **103**, 07C507 (2008).
[15]S. Neusser, G. Duerr, H. G. Bauer, S. Tacchi, M. Madami, G. Woltersdorf, G. Gubbiotti, C. H. Back, and D. Grundler, Phys. Rev. Lett. **105**, 067208 (2010).
[16]H. Ulrichs, B. Lenk, and M. Munzenberg, Appl. Phys. Lett. **97**, 092506 (2010).
[17]S. Tacchi, M. Madami, G. Gubbiotti, G. Carlotti, A. O. Adeyeye, S. Neusser, B. Botters, and D. Grundler, IEEE Trans. Magn. **46**, 1440 (2010).
[18]J. Ding, D. Tripathy, and A. O. Adeyeye, J. Appl. Phys. **109**, 07D304 (2011).
[19]S. Neusser, G. Duerr, S. Tacchi, M. Madami, M. L. Sokolovskyy, G. Gubbiotti, M. Krawczyk, and D. Grundler, Phys. Rev. B **84**, 094454 (2011).
[20]S. Neusser, H. G. Bauer, G. Duerr, R. Huber, S. Mamica, G. Woltersdorf, M. Krawczyk, C. H. Back, and D. Grundler, Phys. Rev. B **84**, 184411 (2011).
[21]R. Zivieri, S. Tacchi, F. Montoncello, L. Giovannini, F. Nizzoli, M. Madami, G. Gubbiotti, G. Carlotti, S. Neusser, G. Duerr, and D. Grundler, Phys. Rev. B **85**, 012403 (2012).
[22]R. Bali, M. Kostylev, D. Tripathy, A. O. Adeyeye, and S. Samarin, Phys. Rev. B **85**, 104414 (2012).
[23]S. Tacchi, B. Botters, M. Madami, J. W. Kłos, M. L. Sokolovskyy, M. Krawczyk, G. Gubbiotti, G. Carlotti, A. O. Adeyeye, S. Neusser, and D. Grundler, Phys. Rev. B **86**, 014417 (2012).
[24]R. Mandal, S. Saha, D. Kumar, S. Barman, S. Pal, K. Das, A. K. Raychaudhuri, Y. Fukuma, Y. Otani, and A. Barman, ACS Nano **6**, 3397 (2012).
[25]D. Kumar, P. Sabareesan, W. Wang, H. Fangohr, and A. Barman, J. Appl. Phys. **114**, 023910 (2013).
[26]M. Donahue and D. G. Porter, OOMMF User's guide, Version 1.0, NIST Interagency Report No. 6376, National Institute of Standard and Technology, Gaithersburg, MD, 1999.
[27]D. Kumar, O. Dmytriiev, S. Ponraj, and A. Barman, J. Phys. D: Appl. Phys. **45**, 015001 (2012).